

Published in final edited form as:

*Inorg Chem.* 2011 December 5; 50(23): 12018–12024. doi:10.1021/ic201479q.

## Modulation of Ligand-field Parameters by Heme Ruffling in Cytochromes C Revealed by EPR Spectroscopy

Mehmet Can<sup>†,§</sup>, Giorgio Zoppellaro<sup>‡,§</sup>, K. Kristoffer Andersson<sup>‡</sup>, and Kara L. Bren<sup>\*†</sup>

<sup>†</sup>Department of Chemistry, University of Rochester, Rochester, New York 14627-0216 USA

<sup>‡</sup>Department of Molecular Biosciences, University of Oslo, Post Office Box 1041, Blindern, Oslo NO-0316, Norway

### Abstract

Electron paramagnetic resonance (EPR) spectra of variants of *Hydrogenobacter thermophilus* cytochrome *c*<sub>552</sub> (*Ht c-552*) and *Pseudomonas aeruginosa* cytochrome *c*<sub>551</sub> (*Pa c-551*) are analyzed to determine the effect of heme ruffling on ligand-field parameters. Mutations introduced at positions 13 and 22 in *Ht c-552* were previously demonstrated to influence hydrogen bonding in the proximal heme pocket and to tune reduction potential ( $E_m$ ) over a range of 80 mV [Michel, L. V.; Ye, T.; Bowman, S. E. J.; Levin, B. D.; Hahn, M. A.; Russell, B. S.; Elliott, S. J.; Bren, K. L., *Biochemistry* **2007**, *46*, 11753–11760]. These mutations are shown here to also increase heme ruffling as  $E_m$  decreases. The primary effect on electronic structure of increasing heme ruffling is found to be a decrease in the axial ligand-field term  $\Delta/\lambda$ , which is proposed to arise from an increase in the energy of the  $d_{xy}$  orbital. Mutations at position 7, previously demonstrated to influence heme ruffling in *Pa c-551* and *Ht c-552*, are utilized to test this correlation between molecular and electronic structure. In conclusion, the structure of the proximal heme pocket of cytochromes *c* is shown to play a role in determining heme conformation and electronic structure.

### Introduction

Iron protoporphyrin IX (heme) is a cofactor found in proteins that carry out electron Heme transfer, oxygen transport and storage, sensing, and a wide range of metabolic processes. Heme *c* is a widely distributed form of heme characterized by covalent attachment to two Cys in a Cys-X-X-Cys-His (CXXCH) motif in which His is an axial ligand to the iron of the heme.<sup>1</sup> His/Met is a common ligand set for heme *c* and is seen in soluble cytochromes *c*, photosynthetic reaction centers, mitochondrial cytochromes *c*<sub>1</sub>, diheme cytochrome *c* peroxidases, and several dehydrogenases and cytochrome *cd*<sub>1</sub> nitrite reductases.<sup>1, 2</sup> Analysis of structures of hemes *c* with His/Met axial ligation reveals that the His imidazole ring is generally oriented along the porphyrin  $\alpha$ - $\gamma$  meso axis (Figure 1A).<sup>3</sup> The axial Met side chain, in contrast, can adopt a number of orientations relative to the heme plane.<sup>4, 5</sup> In some cases, Met fluxionality, a phenomenon that involves rapid interconversion between the *R* and *S* configurations at the Met  $\delta$ S, is observed.<sup>6, 7</sup> Although heme proteins with His/Met axial ligation have been studied extensively using a variety of spectroscopic methods, detailed relationships between active-site structure, *g* values, and associated ligand-field components

\*To whom correspondence should be addressed. bren@chem.rochester.edu.

§Contributed equally

Supporting Information Available: Detailed description of the determination of ligand-field parameters from *g*-values and their errors, error distribution in the *g*-tensor and calculated ligand-field parameters (5 Tables), an illustration of the error analysis procedure and an expansion of the high-field region of EPR spectra of the protein variants with fits (2 Figures). This material is available free of charge via the Internet at <http://pubs.acs.org>.

determined by spectroscopic methods such as EPR, Mössbauer, MCD, and NMR remain elusive for this important class of proteins.<sup>8–10</sup>

In contrast with heme with His/Met axial ligation, for heme with His/His axial ligation, relationships between heme active-site structure,  $g$  values, and NMR hyperfine shifts are well defined.<sup>12–14</sup> In particular, it has been established that the angle between the two axial His imidazole planes plays a major role in determining the  $g$ -tensor and ligand-field parameters. If the two axial His planes are oriented perpendicular or nearly so to each other, a large  $g_{\max}$  value ( $g_{\max} > 3.3$ ) and an axial EPR spectrum results, whereas a relatively small angle between the axial ligand planes yields a lower  $g_{\max}$  value and a rhombic spectrum.<sup>12</sup> The spin-orbit coupling constant ( $\lambda$ ) and the experimentally observed  $g$  values can be used to estimate the rhombic ( $V$ ) and axial ( $\Delta$ ) ligand-field terms,<sup>15</sup> and thus the relative energies of the iron(III) d-orbitals (Figure 2); the ratio  $V/\Delta$  is used as an indicator of the system's rhombicity. The axial His imidazole plane orientations also correlate with the NMR hyperfine shifts of heme substituents, and thus for proteins with His/His axial ligation, interrelationships among properties of NMR spectra, EPR spectra, and active-site structure are well established.

Progress toward understanding how EPR parameters reflect properties of heme with His/Met axial ligation was made in a study of a series of cytochrome *c* variants in which linear relationships were identified between the average heme methyl chemical shift ( $\langle\delta\rangle$ ) determined from NMR and both  $g_{\max}$  and  $V/\Delta$  determined from EPR. A structural basis for the observed changes was not established, but it was proposed to be associated with heme conformation, axial ligand strength and orientation, or a combination of these factors.<sup>9</sup> In the present study, to better define the relationship between molecular and electronic structure of heme *c* with His/Met axial ligands, we report an analysis of EPR data on a series of mutants of small, soluble bacterial cytochromes *c*. The proteins targeted, *Hydrogenobacter thermophilus* cytochrome *c*<sub>552</sub> (*Ht c*-552), and *Pseudomonas aeruginosa* cytochrome *c*<sub>551</sub> (*Pa c*-551), constitute a homologous pair with 57% sequence identity. Mutations in these proteins have been made at positions 7, 13, and 22, which are located near the CXXCH heme attachment site (residues 12–16; Figure 3). Mutation of residue 7 has been shown to influence heme ruffling in both proteins,<sup>11, 16, 17</sup> and mutations of residues 13 and 22 have been shown to affect the His-Fe(III) interaction and are proposed to influence heme ruffling.<sup>18, 19</sup>

Ruffling is typically the dominant mode of out-of-plane distortion for heme *c*,<sup>21</sup> and can be envisioned as twisting along the Fe-N(pyrrole) bonds in alternate directions (Figure 4).<sup>22</sup> The X-ray crystal structure of the Phe7Ala mutant of *Pa c*-551 (*PaF7A*)<sup>17</sup> indicates an increase in the out-of-plane displacement along the ruffling coordinate of 0.4 Å measured using normal coordinate structural decomposition analysis<sup>16, 22</sup> of the X-ray crystal structures of *Pa c*-551<sup>11</sup> and *PaF7A*.<sup>17</sup> The basis for the change in ruffling may be the shortening of the hydrogen bond between the residue 7 backbone carbonyl oxygen and Cys12 amide NH in *PaF7A* relative to wild-type.<sup>16, 17</sup> Conversely, NMR analysis has revealed that the A7F mutation in *Ht c*-552 decreases heme ruffling by ~0.1 Å.<sup>16</sup> The M13V and K22M mutations in *Ht c*-552 have been demonstrated to increase His-Fe(III) bond strength, and have been proposed although not proven to influence heme ruffling.<sup>18, 19</sup> These variants span an 80-mV range of  $E_m$ , corresponding to an increase in His-Fe(III) bond strength as  $E_m$  decreases (*Ht c*-552:  $236 \pm 2$  mV, *HtK22M*:  $199 \pm 1$ ; *HtM13V*:  $177 \pm 1$  mV; *HtM13V/K22M*:  $155 \pm 2$  mV).<sup>18</sup> Position 7, 13, and 22 variants of *Ht c*-552 and position 7 variants of *Pa c*-551 are used here for a detailed investigation of the effects of His-Fe(III) bonding and heme ruffling on the electronic structure of heme proteins with His-Met axial ligation as revealed by EPR spectroscopy.

## Experimental Section

### Protein Expression and Purification

Expression of *Ht c-552*,<sup>23</sup> *HtM13V*, *HtK22M*, *HtM13V/K22M*,<sup>18</sup> and *HtA7F16* was in *E. coli* BL21(DE3)Star (Invitrogen) containing pEC86 for overexpression of the *E. coli* cytochrome *c* maturation genes<sup>24</sup> and the appropriate cytochrome *c* expression plasmid harboring the cytochrome structural gene with a signal sequence. The expression plasmids for *Ht c-552* and variants are based on pET17b (Amp<sup>r</sup>) (Novagen) and utilize a modified N-terminal signal sequence from *Thiobacillus versutus* cytochrome *c*<sub>550</sub> to direct secretion of the apoprotein to periplasm for maturation.<sup>25</sup> Purification was as described.<sup>18</sup> Expression of *Pa c-551* and *PaF7A* also was in *E. coli* BL21(DE3)Star and used a pET17b-based plasmid containing the *Pa c-551* gene along with its native signal sequence<sup>20, 26</sup> in addition to pEC86. The QuikChange II site-directed mutagenesis kit (Stratagene) was used to prepare the F7A variant of *Pa c-551*. Purification of *Pa c-551* and *PaF7A* was as described<sup>27</sup> and yielded 15–20 mg protein/L of medium.

### EPR Spectroscopy

EPR measurements on cytochrome *c* variants (protein concentration 200–300 μM, 50 mM HEPES, pH 7.5) were carried out in a dual-band X-cavity on a Bruker Elexsys 500E spectrometer characterized by a cavity quality factor ( $Q$ ) > 4000 and equipped with a He–flow cryostat (ESR 900, Oxford Instruments). Spectra were recorded at a temperature of 9.0 ± 1.0 K and a microwave frequency of 9.663(8) GHz. To avoid saturation effects, the microwave power was calibrated for each protein sample and all EPR spectra reported here were obtained with a microwave power well below  $P_{1/2}$ . Microwave powers used were: *Ht c-552*: 1.0 mW, *HtK22M*: 6.4 mW, *HtM13V*: 3.2 mW, *HtMI3V/K22M*: 0.63 mW, *Pa c-551*: 1.0 mW, *PaF7A*: 3.6 mW. Spectra were collected with a modulation amplitude of 0.7 mT, modulation frequency of 100 KHz, gain of 57 dB, sweep time of 168–335 sec, and time constant of 82–164 msec. For each sample, 2–6 scans were accumulated and averaged. EPR spectra were baseline corrected by subtraction of a scan of the cavity and the EPR tube containing buffer (keeping the same filling volume) recorded under identical conditions. The EPR simulation platform XSophe (ver. 1.1.3) and XeprView (ver. 1.2b.33) software were provided by Bruker.<sup>28</sup>

### Determination of Ligand-Field Parameters

The ligand–field correlation analysis employed in this work follows the formalism introduced by Griffith<sup>29, 30</sup> and developed by Taylor.<sup>15</sup> Axial ( $\Delta/\lambda$ ) and rhombic ( $V/\lambda$ ) ligand-field terms (Figure 2) were determined from the experimental  $g$  values according to the following equations:

$$\frac{V}{\lambda} = \frac{E_{yz}}{\lambda} - \frac{E_{xz}}{\lambda} = \frac{g_{xx}}{g_{zz} + g_{yy}} + \frac{g_{yy}}{g_{zz} - g_{xx}} \quad (1)$$

$$\frac{\Delta}{\lambda} = \frac{E_{yz}}{\lambda} - \frac{E_{xy}}{\lambda} - \frac{V}{2\lambda} = \frac{g_{xx}}{g_{zz} + g_{yy}} + \frac{g_{zz}}{g_{yy} - g_{xx}} - \frac{V}{2\lambda} \quad (2)$$

Use of these equations requires that the normalization condition holds:<sup>15, 31</sup>

$$g_{xx}^2 + g_{yy}^2 + g_{zz}^2 + g_y g_z - g_x g_z - g_x g_y - 4(g_{zz} + g_{yy} - g_{xx}) = 0 \quad (3)$$

The spectra of the cytochrome *c* variants studied in this work fulfill the conditions expressed by Eq. 3. The calculated orbital coefficient values (*a*, *b*, *c*) and details of the procedure employed for estimation of errors in the ligand-field terms are provided in the Supporting Information.

## Results

The experimentally determined *g*-tensor components and the derived ligand-field terms for the proteins in this study are presented in Table 1. The EPR spectra of all of the protein variants exhibit resonance signals consistent with low-spin (*S* = 1/2) ferric heme with a ( $d_{xy}$ )<sup>2</sup> ( $d_{xz}$ ,  $d_{yz}$ )<sup>3</sup> electronic configuration and moderate rhombic distortion (Figure 5, Figure S2, Table 1). For the *Ht c*-552 position 13 and 22 variants, a linear relationship between *V*/ $\lambda$  and  $\Delta/\lambda$  values and  $E_m$  (Figure 6) is observed. The position 13 and 22 variants of *Ht c*-552 show a linear increase in the rhombic term *V*/ $\lambda$  and decrease in the axial term  $\Delta/\lambda$  as  $E_m$  decreases; both factors contribute to the increase of rhombicity (*V*/ $\Delta$ ) over the series. However, the variation in *V*/ $\lambda$  values is relatively small, thus changes in  $\Delta/\lambda$  dominate the *d*-orbital distribution. *HtA7F*, in contrast, shows minimal change in its EPR spectrum relative to wild-type.<sup>16</sup> *PaF7A* exhibits a slightly higher rhombicity in comparison with *Pa c*-551, but with a larger change in  $\Delta/\lambda$  than in *V*/ $\lambda$  (Table 1).

## Discussion

The axial His-Fe(III) bond strength is proposed to be related to the amount of anionic (histidinate) character of the axial His which influences the reduction potential of peroxidases<sup>32</sup> and cytochromes.<sup>19</sup> For a given His orientation, histidinate character also is related to the strength of the hydrogen bond between the axial His  $\delta$ 1 NH and its hydrogen bond acceptor, which in cytochromes *c* is a proline carbonyl. Because a stronger bond from His to Fe(III) stabilizes the higher oxidation state, reduction potential will decrease with increasing His-Fe(III) bond strength. Accordingly, the position 13 and 22 mutants of *Ht c*-552 have been shown to have a stronger His-Fe(III) bond as  $E_m$  is lowered. Note that these mutations have been shown to have a minimal effect on the properties of the Fe(II) state of *Ht c*-552.<sup>19</sup> The His-Fe(III) and Met-Fe(III) interactions have significant  $\sigma$ -bonding character involving the Fe  $d_{z^2}$  orbital. The predicted effect of enhanced  $\sigma$ -bonding between axial ligands and the iron is to increase the energy of the  $d_{z^2}$  orbital, as illustrated in Figure 7A. The Fe  $d_{xz}$  and  $d_{yz}$  orbitals exhibit  $\pi$ -interactions with the Met  $\delta$ S lone pair, the porphyrin  $\pi$ -system, and the His  $\pi$  orbitals. Enhancing  $\pi$  interactions with the Fe  $d_{xz}$  and  $d_{yz}$  orbitals will raise their energies as shown in Figure 7B. Preferential destabilization of either the  $d_{xz}$  or  $d_{yz}$  orbital as Fe(III)-ligand  $\pi$ -bonding depends on the orientations of the axial ligands relative to the heme *x*, *y* plane.

### His-Fe(III) Bonding

Analysis of the EPR spectra of the position 13 and 22 variants reveals that the rhombic term *V*/ $\lambda$ , reflecting the difference in energy between the  $d_{xz}$  and  $d_{yz}$  orbitals, shows a small increase across the series: *Ht c*-552 < *HtK22M* < *HtM13V* < *HtM13V/K22M* (i.e., from higher to lower  $E_m$ ), whereas  $\Delta/\lambda$  decreases. Can these changes be attributed to the effects of increasing His-Fe(III) bond strength that was previously established?<sup>19</sup> The axial His is nearly aligned with the  $\alpha,\gamma$ -meso carbons of the heme (Figure 1A).<sup>11, 17</sup> Changes in the Fe(III)-His bond strength observed across this series thus are expected to affect the  $d_{xz}$  and  $d_{yz}$  energies similarly. The small amount of change in *V*/ $\lambda$  with increasing His-Fe(III) bond

strength is consistent with the His being nearly, but not precisely, aligned with the  $\alpha,\gamma$ -meso carbons (Figure 1A), because increasing the bond strength will result in more overlap between the  $\pi$ -system of the His with *both* the  $d_{xz}$  and  $d_{yz}$  orbitals, raising both energies to a similar extent. As a result, an increase in the axial His-Fe(III) interaction in this system is predicted to increase the axial term  $\Delta/\lambda$  but exert little change on the rhombic term  $V/\lambda$ . However, we observe a *decrease* in the axial term with increasing His-Fe(III) bond strength. To explain this trend, we next consider the effects of variation of heme ruffling on electronic structure.

### Heme Ruffling

The *Pa c-551/PaF7A* and the *Ht c-552/HtA7F* wild-type/mutant pairs are valuable for examining the effect of heme ruffling on ligand-field parameters as they exhibit changes in ruffling that have been established previously.<sup>16</sup> EPR results for the *Ht c-552/HtA7F* pair and for *Pa c-551* were reported elsewhere<sup>9, 16</sup> and the EPR spectrum for *PaF7A* is reported here. Comparison of EPR results for *Pa c-551* and *PaF7A* shows that the rhombic term  $V/\lambda$  does not change upon mutation whereas the axial term  $\Delta/\lambda$  decreases significantly for the more ruffled F7A mutant. In Taylor's model for the  $(d_{xy})^2(d_{xz},d_{yz})^3$  configuration,  $\Delta/\lambda = 1/2 (E_{xz} + E_{yz}) - E_{xy}$ , hence a decrease in  $\Delta/\lambda$  reflects either 1) a decrease in the  $d_{xz},d_{yz}$  orbital energies ( $E_{xz}$  and  $E_{yz}$ ) relative to  $E_{xy}$  or 2) an increase in  $E_{xy}$  relative to  $E_{xz}$  and  $E_{yz}$ ; a combination of these effects also is possible. In Taylor's treatment, the  $S = 1/2$  wavefunctions ( $|+\rangle, |-\rangle$ ) are described as a weighted admixture of the  $d_{xy}$ ,  $d_{xz}$ , and  $d_{yz}$  orbitals with orbital coefficients  $a$ ,  $b$  and  $c$ :

$$\begin{aligned} |+\rangle &= a|d_{yz}^+\rangle - ib|d_{xz}^+\rangle - c|d_{xy}^-\rangle \\ |-\rangle &= -a|d_{yz}^-\rangle - ib|d_{xz}^-\rangle - c|d_{xy}^+\rangle \end{aligned}$$

By utilizing the normalization condition  $\Sigma(a)^2 + (b)^2 + (c)^2 = 1.00 \pm 0.01$  we can determine the coefficients for the  $d_{xy}$ ,  $d_{xz}$ , and  $d_{yz}$  components of the three-orbitals-one-hole wavefunctions. The result for *Pa c-551* is that the spin functions contain ~86%  $d_{yz}$ , 12%  $d_{xz}$  and 2%  $d_{xy}$  while in *PaF7A* they contain ~85%  $d_{yz}$ , 12%  $d_{xz}$  and 3%  $d_{xy}$ . Thus the contributions of both the  $d_{yz}$  and  $d_{xy}$  orbitals are altered by mutation, although the  $d_{xy}$  has the larger relative change.

The influence of heme conformation on the d orbital energies is mediated by interactions between the filled  $3e(p)$  porphyrinate orbital and the  $d_{xz}$  and  $d_{yz}$  ( $d(\pi)$ ) metal orbitals, and, if the macrocycle is ruffled, by interactions between the filled  $3a_{2u}(\pi)$  porphyrinate orbital and the  $d_{xy}$  orbital (Figure 8). Those interactions depend on the relative energies of the  $d(\pi)$  metal and  $e(\pi)$  macrocycle frontier orbitals. Thus, the smaller axial term ( $\Delta/\lambda$ ) may indicate either 1) a weakening of the  $3e(\pi)$ - $d(\pi)$  interaction in *PaF7A* with respect to *Pa c-551* to lower  $E_{yz}$ , or 2) an enhanced interaction between  $3a_{2u}(\pi)$  and  $d_{xy}$  to raise  $E_{xy}$ ; a combination of these factors also is possible. From CW-EPR data alone we cannot determine which of these is the major contributor. In a recent DFT study, however, an increase in heme ruffling in low-spin heme with His/Met axial ligation was predicted to increase the energies of all three  $t_{2g}$ -derived orbitals, although the effect was much more pronounced for  $d_{xy}$ . The DFT predictions were validated by NMR spectroscopy performed on *Ht c-552* and on *Ht-A7F*; the results demonstrated that the mutation decreases heme ruffling.<sup>16</sup>

In contrast with the *Pa c-551/PaF7A* pair, *HtA7F* displays no significant difference in ligand-field terms from *Ht c-552*. EPR data are consistent with a small increase in  $\Delta/\lambda$  for *HtA7F*, however, the change is within the margin of error. The small change in  $\Delta/\lambda$  for *HtA7F* relative to wild-type may be attributed to the very small change in ruffling seen between these proteins (~0.1 Å, determined by NMR)<sup>16</sup> relative to the *Pa c-551/PaF7A* pair

(~0.4 Å, measured from crystal structures).<sup>11, 17</sup> Thus, EPR may be sensitive to moderate or large heme ruffling differences between hemes with His/Met axial ligation although it may not reflect small heme ruffling changes that are detectable by NMR.<sup>16</sup>

As noted above,  $\Delta/\lambda$  decreases across the series *Ht c-552* > *HtK22M* > *HtM13V* > *HtM13V/K22M* as  $E_m$  decreases, although an increase in the axial His-Fe(III) bond strength is predicted to result in an increase in the axial term  $\Delta/\lambda$ . This result thus supports the hypothesis that heme ruffling increases across this series of variants with decreasing  $E_m$ , resulting in a higher energy for  $d_{xy}$  and a lower  $\Delta/\lambda$ . The average value of the heme methyl chemical shifts shows an established trend with a change in ruffling, and the average heme methyl <sup>1</sup>H chemical shift decreases across the series of position 13 and 22 *Ht c-552* mutants as  $E_m$  decreases, consistent with an increase in heme ruffling.<sup>16, 19, 33</sup> The average heme methyl chemical shift also is sensitive to axial ligand donor properties. As the axial His becomes a better donor (more histidinate character), the average heme methyl shift moves upfield as a result of a decrease in porphyrin-to-Fe( $\pi$ ) spin delocalization as the His-to-Fe(III)  $\sigma$ -interaction increases.<sup>34</sup> Thus both an increase in heme ruffling and in His-donor properties may be causes of the observed trend in heme methyl chemical shifts. However, as enhanced His-Fe(III) bonding is predicted to increase  $\Delta/\lambda$ , we conclude that the differences observed in the EPR spectra among the variants arise primarily from differences in ruffling.

### Structural Basis for Ruffling and Functional Implications

A clue to the structural basis for the trend in heme ruffling in the position 13 and 22 mutants may be found in the previously-reported effects of these mutations on the CXXCH pentapeptide. The M13V and K22M mutations were previously proposed to enhance packing on the proximal (axial His) side of the heme. Accordingly, these mutations were found to increase the rigidity of the proximal heme pocket. The backbone HN protons of Cys15 and His16 hydrogen bond with the Cys12 carbonyl oxygen (Figure 9), and the persistence of these interactions has been probed by hydrogen-deuterium exchange NMR.<sup>18</sup> In *HtM13V*, *HtK22M*, and *HtM13V/K22M*, the backbone HN protons of Cys15 and His16 show increased protection from exchange with solvent, with amount of protection generally increasing as  $E_m$  decreases.<sup>18</sup> This result is interpreted to indicate a more locally stable or rigid CXXCH peptide backbone in the lower-potential mutants with enhanced polypeptide packing near the axial His. Studies of microperoxidase heme peptides derived from horse cytochrome *c* have previously demonstrated that strengthening hydrogen bonding within the CXXCH segment enhances heme ruffling.<sup>35</sup> Thus, we propose that enhanced hydrogen bonding within the CXXCH pentapeptide backbone contributes to increasing heme ruffling in these mutants.

Across the series of position 13 and 22 mutants, moving from higher to lower  $E_m$ , we propose that both heme ruffling and His-Fe(III) bond strength are enhanced. Might axial bond strength and heme ruffling be linked to each other? The effect of heme ruffling on axial bond strength has been explored in a study of ligand-binding affinities of ferric myoglobins reconstituted with heme derivatives showing different amounts of ruffling. Heme distortion is proposed to increase the Fe(III)-His bond strength in that work.<sup>36</sup> In contrast, DFT calculations on a Met-His-coordinated heme predict a negligible effect of heme ruffling on Fe(III)-His bond length with a bond length change of less than 0.001 Å upon a change of ruffling of 0.7 Å (see supporting information of ref. 16). However, it is possible that protein structure-related factors affecting heme ruffling also directly affect the Fe(III)-His bond strength, or that changes in ruffling and bond strength are otherwise related to each other. In contrast with the analyses of Fe(III)-His bonding, a study of dioxygen binding to the highly distorted ferrous heme in *Methanosarcina acetivorans* protoglobin indicates that out-of-plane distortions decrease dioxygen affinity, whereas in-plane distortions may increase or decrease affinity.<sup>37</sup> Consistent with the conclusions on

protoglobin, a study of the effect of heme ruffling on ligand-binding to *Thermoanaerobacter tencongenensis* heme nitric oxide/oxygen binding domain suggests that flattening of the heme increases the proximal bond strength of the Fe(II)-O<sub>2</sub> complex.<sup>38</sup> How ruffling affects axial ligand interactions remains a question for further research, but likely depends on heme oxidation state, electronic structure, and the nature of the ligand(s).

In a previous study, changes in heme ruffling were proposed to influence whether highly axial low-spin (HALS)-type (high  $g_{\max}$ ) or rhombic EPR spectra of Met-His coordinated cytochromes *c* were observed.<sup>9</sup> The analysis here indicates a limited effect of heme ruffling on  $g_{\max}$ . A  $g_{\max}$  value difference of only 0.05 is observed between *Pa c-551* and *PaF7A* despite the 0.4-Å change in the heme ruffling; the difference between the  $g_{\max}$  values of wild-type *Ht c-552* and *HtM13V/K22M*, the variant with the greatest difference in  $E_m$  from wild-type, is only 0.06. Thus, changes exerted on EPR spectra by heme ruffling in these systems can not be the sole basis for the large range of  $g_{\max}$  values exhibited by cytochromes.<sup>10</sup> However, it is notable that *Bacillus pasteurii* cytochrome *c*<sub>553</sub> has a low amount of ruffling for a cytochrome *c* (0.36 Å)<sup>39</sup> and a large  $g_{\max}$  signal (3.36).<sup>8</sup>

There has been considerable interest in the question of the functional relevance of covalent heme attachment in cytochromes *c*.<sup>1, 40, 41</sup> One proposal is that covalent attachment provides means by which redox potential may be tuned, as hemes *c* display a wider range of potentials in nature than hemes *b*, which bind the polypeptide through coordinate bonds and noncovalent interactions.<sup>1, 42</sup> The observation that mutations in and near the CXXCH motif influence heme ruffling and His-Fe(III) bonding, supports the hypothesis that covalent attachment, the identity of the variable residues within this motif, and interactions with this motif influence heme conformation, and thus heme *c* redox potential.

## Supplementary Material

Refer to Web version on PubMed Central for supplementary material.

## Acknowledgments

This work was supported by The National Institutes of Health (NIH) of the United States of America Grant GM63170 (K.L.B.), the Research Council of Norway Grant 177661/V30 (K.K.A.). GZ thanks the support from the PEOPLE Marie Curie actions Intra European Fellowship within the 7<sup>th</sup> European Community Framework Program (PIEF-GA-2009-235237).

## References

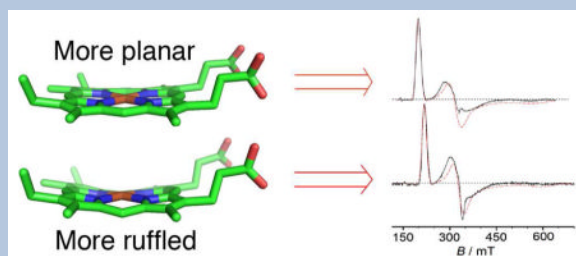
1. Bowman SEJ, Bren KL. Nat Prod Rep. 2008; 25:1118–1130. [PubMed: 19030605]
2. Reedy CJ, Elvekrog MM, Gibney BR. Nucleic Acids Res. 2008; 36:D307–D313. [PubMed: 17933771]
3. Fufezan C, Zhang J, Gunner MR. Proteins. 2008; 73:690–704. [PubMed: 18491383]
4. Senn H, Keller RM, Wüthrich K. Biochem Biophys Res Commun. 1980; 92:1362–1369. [PubMed: 6245651]
5. Moore, GR.; Pettigrew, GW. Cytochromes *c*; Evolutionary, Structural, and Physicochemical Aspects. Springer-Verlag; Berlin: 1990.
6. Zhong L, Wen X, Rabinowitz TM, Russell BS, Karan EF, Bren KL. Proc Natl Acad Sci USA. 2004; 101:8637–8642. [PubMed: 15161973]
7. Bren KL, Kellogg JA, Kaur R, Wen X. Inorg Chem. 2004; 43:7934–7944. [PubMed: 15578827]
8. Zoppellaro G, Teschner T, Harbitz E, Schuenemann V, Karlsen S, Arciero DM, Ciurli S, Trautwein AX, Hooper AB, Andersson KK. ChemPhysChem. 2006; 7:1258–1267. [PubMed: 16688708]
9. Zoppellaro G, Harbitz E, Kaur R, Ensign AA, Bren KL, Andersson KK. J Am Chem Soc. 2008; 130:15348–15360. [PubMed: 18947229]

10. Zoppellaro G, Bren KL, Ensign AA, Harbitz E, Kaur R, Hersleth HP, Ryde U, Hederstedt L, Andersson KK. *Biopolymers*. 2009; 91:1064–1082. [PubMed: 19536822]
11. Matsuura Y, Takano T, Dickerson RE. *J Mol Biol*. 1982; 156:389–409. [PubMed: 6283101]
12. Walker FA. *Chem Rev*. 2004; 104:589–615. [PubMed: 14871136]
13. Bertini I, Luchinat C, Parigi G, Walker FA. *J Biol Inorg Chem*. 1999; 4:515–519. [PubMed: 10555585]
14. Shokhirev NV, Walker FA. *J Biol Inorg Chem*. 1998; 3:581–594.
15. Taylor CPS. *Biochim Biophys Acta*. 1977; 491:137–149. [PubMed: 191085]
16. Liptak MD, Wen X, Bren KL. *J Am Chem Soc*. 2010; 132:9753–9763. [PubMed: 20572664]
17. Borgia A, Bonivento D, Travaglini-Allocatelli C, Di Matteo A, Brunori M. *J Biol Chem*. 2006; 281:9331–9336. [PubMed: 16452476]
18. Michel LV, Ye T, Bowman SEJ, Levin BD, Hahn MA, Russell BS, Elliott SJ, Bren KL. *Biochemistry*. 2007; 46:11753–11760. [PubMed: 17900177]
19. Bowman SEJ, Bren KL. *Inorg Chem*. 2010; 49:7890–7897. [PubMed: 20666367]
20. Travaglini-Allocatelli C, Gianni S, Dubey VK, Borgia A, Di Matteo A, Bonivento D, Cutruzzolà F, Bren KL, Brunori M. *J Biol Chem*. 2005; 280:25729–25734. [PubMed: 15883159]
21. Hobbs JD, Shelnett JA. *J Protein Chem*. 1995; 14:19–25. [PubMed: 7779259]
22. Jentzen W, Song XZ, Shelnett JA. *J Phys Chem B*. 1997; 101:1684–1699.
23. Karan EF, Russell BS, Bren KL. *J Biol Inorg Chem*. 2002; 7:260–272. [PubMed: 11935350]
24. Arslan E, Schulz H, Zufferey R, Kunzler P, Thöny-Meyer L. *Biochem Biophys Res Commun*. 1998; 251:744–747. [PubMed: 9790980]
25. Fee JA, Chen Y, Todaro TR, Bren KL, Patel KM, Hill MG, Gomez-Moran E, Loehr TM, Ai JY, Thony-Meyer L, Williams PA, Stura E, Sridhar V, McRee DE. *Protein Sci*. 2000; 9:2074–2084. [PubMed: 11152119]
26. Wen X, Bren KL. *Inorg Chem*. 2005; 44:8587–8593. [PubMed: 16271000]
27. Russell BS, Zhong L, Bigotti MG, Cutruzzolà F, Bren KL. *J Biol Inorg Chem*. 2003; 8:156–166. [PubMed: 12459911]
28. Hanson GR, Gates KE, Noble JC, Griffin M, Mitchell A, Benson S. *J Inorg Biochem*. 2004; 98:903–916. [PubMed: 15134936]
29. Griffith JS. *Nature*. 1957; 180:30–31. [PubMed: 13451631]
30. Griffith JS. *Mol Phys*. 1971; 21:135–139.
31. Castner TJ Jr. *Phys Rev*. 1959; 115:1506–1515.
32. Poulos TL. *J Biol Inorg Chem*. 1996; 1:356–359.
33. Shokhireva TK, Shokhirev NV, Berry RE, Zhang HJ, Walker FA. *J Biol Inorg Chem*. 2008; 13:941–959. [PubMed: 18458965]
34. Chacko VP, Lamar GN. *J Am Chem Soc*. 1982; 104:7002–7007.
35. Ma JG, Vanderkooi JM, Zhang J, Jia SL, Shelnett JA. *Biochemistry*. 1999; 38:2787–2795. [PubMed: 10052950]
36. Neya S, Suzuki M, Hoshino T, Ode H, Imai K, Komatsu T, Ikezaki A, Nakamura M, Furutani Y, Kandori H. *Biochemistry*. 2010; 49:5642–5650. [PubMed: 20536131]
37. Bikiel DE, Forti F, Boechi L, Nardini M, Javier Luque F, Martí MA, Estrin DA. *J Phys Chem B*. 2010; 114:8536–8543. [PubMed: 20524694]
38. Olea C, Boon EM, Pellicena P, Kuriyan J, Marletta MA. *ACS Chem Biol*. 2008; 3:703–710. [PubMed: 19032091]
39. Benini S, Gonzalez A, Rypniewski WR, Wilson KS, Van Beeumen JJ, Ciurli S. *Biochemistry*. 2000; 39:13115–13126. [PubMed: 11052663]
40. Stevens JM, Daltrop O, Allen JWA, Ferguson SJ. *Acc Chem Res*. 2004; 37:999–1007. [PubMed: 15609992]
41. Allen JWA, Barker PD, Daltrop O, Stevens JM, Tomlinson EJ, Sinha N, Sambongi Y, Ferguson SJ. *Dalton T*. 2005:3410–3418.
42. Zheng Z, Gunner MR. *Proteins*. 2009; 75:719–734. [PubMed: 19003997]



### Synopsis

Analysis of EPR spectra of cytochrome *c* variants in which proximal heme pocket residues are mutated reveals a relationship between  $g$  values and heme ruffling. The primary effect of increasing heme ruffling is found to be a decrease in the axial ligand-field term  $\Delta/\lambda$ , proposed to arise from an increase in the energy of the  $d_{xy}$  orbital. Thus, proximal heme pocket structure affects heme conformation and electronic structure.



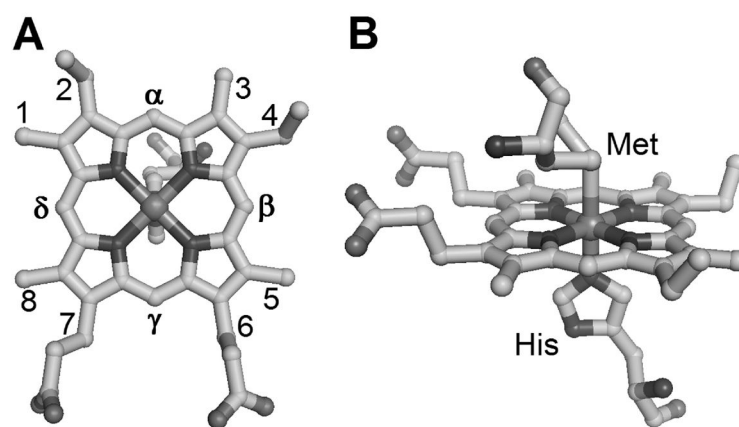


**Figure 1.** Active-site structure of *Pseudomonas aeruginosa* cytochrome c<sub>551</sub> (PDB: 351C<sup>11</sup>) showing (A) Fisher numbering system and axial His orientation and (B) Met and His axial ligands

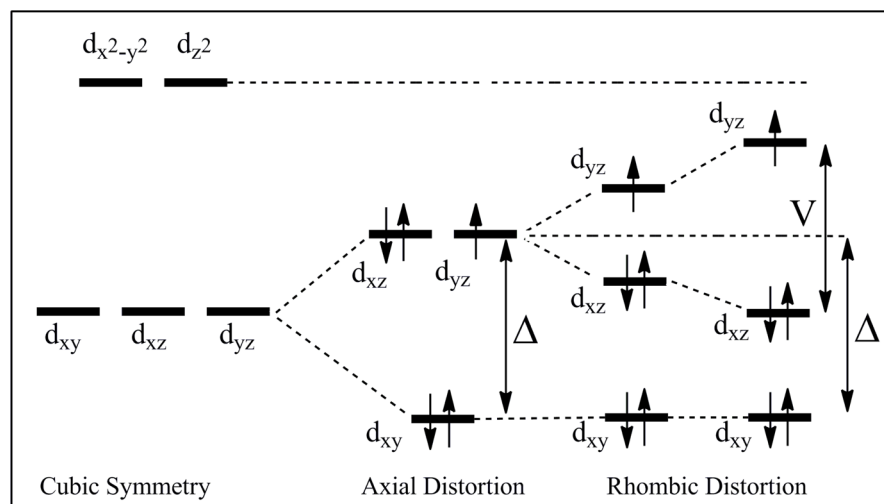


**Figure 2.** Energy diagram of the d-orbitals for the low-spin ferric heme *c* ( $S = 1/2$ ) with  $(d_{xy})^2(d_{xz})^2(d_{yz})^1$  orbital occupancy. The axial ( $\Delta$ ) and rhombic ( $V$ ) ligand-field parameters are shown.

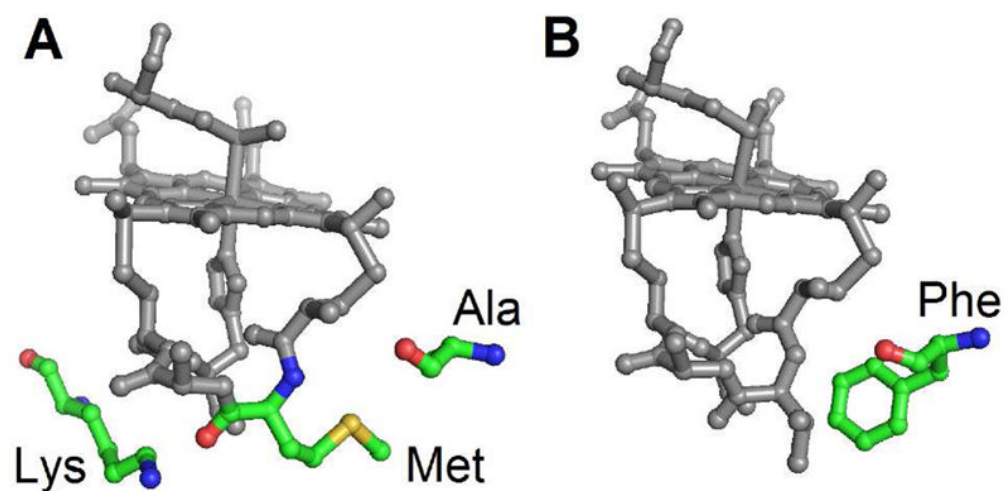


**Figure 3.** Mutation sites in this study. A) Ala7, Met13, and Lys22, shown in *Ht c-552* (PDB: 1YNR<sup>20</sup>) B) Phe7, shown in *Pa c-551* (PDB: 351C<sup>11</sup>). Residue 13 and 22 mutants of *Ht c-552*, and residue 7 mutants of both proteins, are analyzed herein.

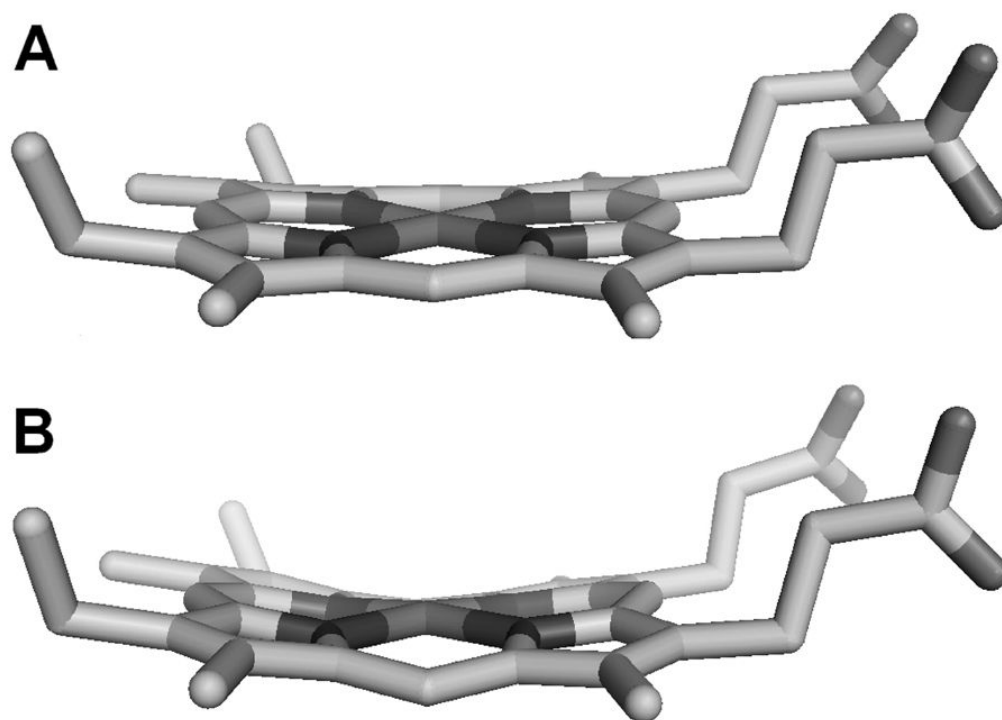


**Figure 4.** Structure of the heme from A) *Pa c-551* (PDB: 351C),<sup>11</sup> 0.49 Å ruffling, and B) *PaF7A* (PDB: 2EXV),<sup>20</sup> 0.86 Å ruffling. Normal coordinate structure decomposition<sup>22</sup> was used to evaluate amount of ruffling which is expressed as the amount of displacement of nuclei along the ruffling coordinate.

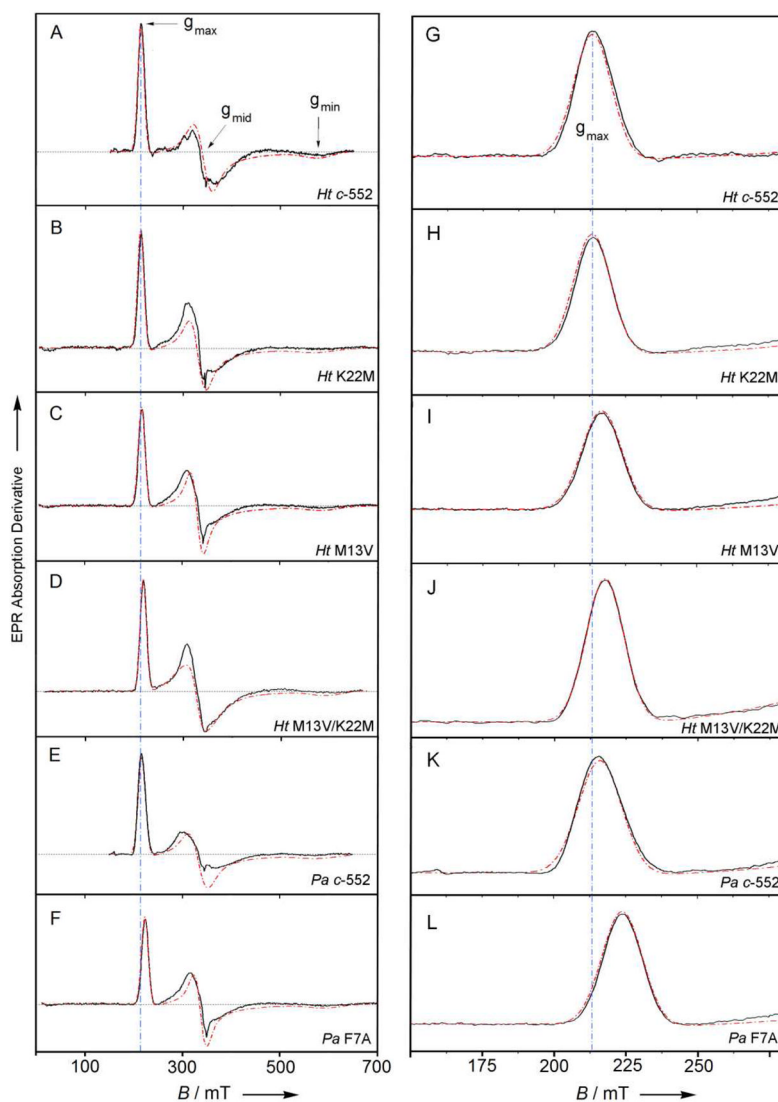


**Figure 5.** X-band EPR spectra of variants of *Ht c-552* and *Pa c-551*: (A,G) *Ht c-552*, (B,H) *HtK22M*, (C,I) *HtM13V*, (D,J) *HtMI3V/K22M*, (E,K) *Pa c-551*, (F,L) *PaF7A*. Sample concentration was 200–300  $\mu\text{M}$  protein in 50 mM HEPES, pH 7.5. Measurements were performed at a temperature of  $9.0 \pm 1.0$  K. The dashed red lines represent simulated EPR envelopes. The dashed blue line is a guide to the eye and indicates the  $g_{\text{max}}$  value for *Ht-c552*. Panels G-L are expansions of the  $g_{\text{max}}$  line.

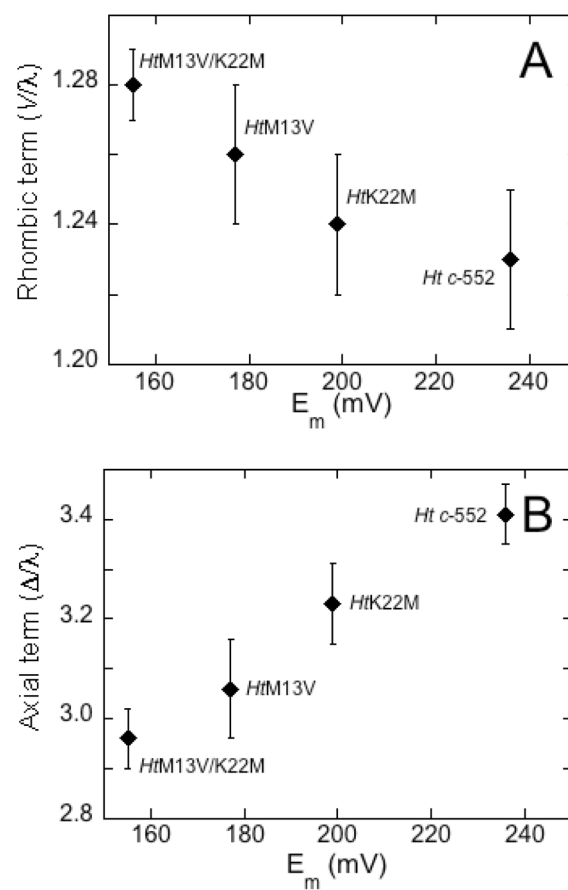


**Figure 6.** Correlation between midpoint potentials and A)  $V/\lambda$ , B)  $\Delta\lambda$ , for *Ht c-552* and its position 13 and 22 variants.

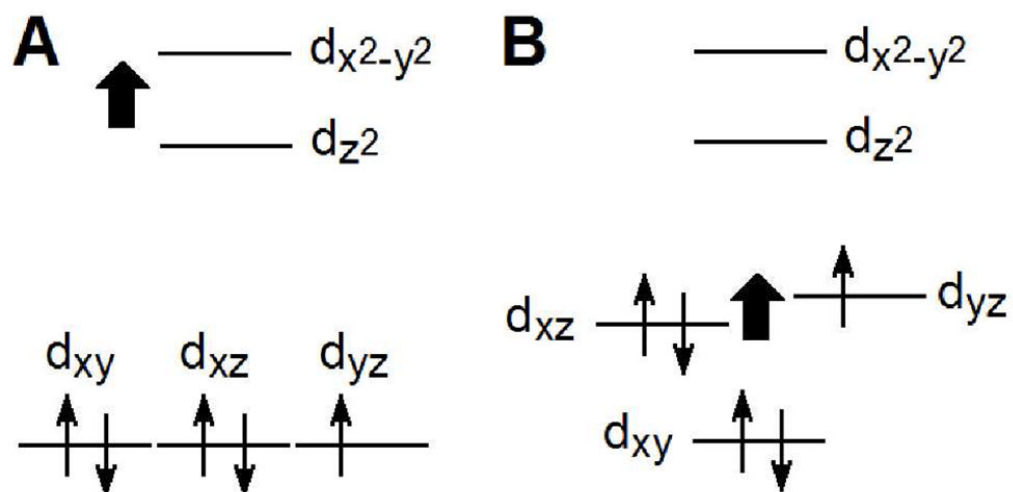


**Figure 7.** Effects of enhanced A)  $\sigma$  donation and B)  $\pi$  donation to iron on the relative energies of the Fe(III) d orbitals.



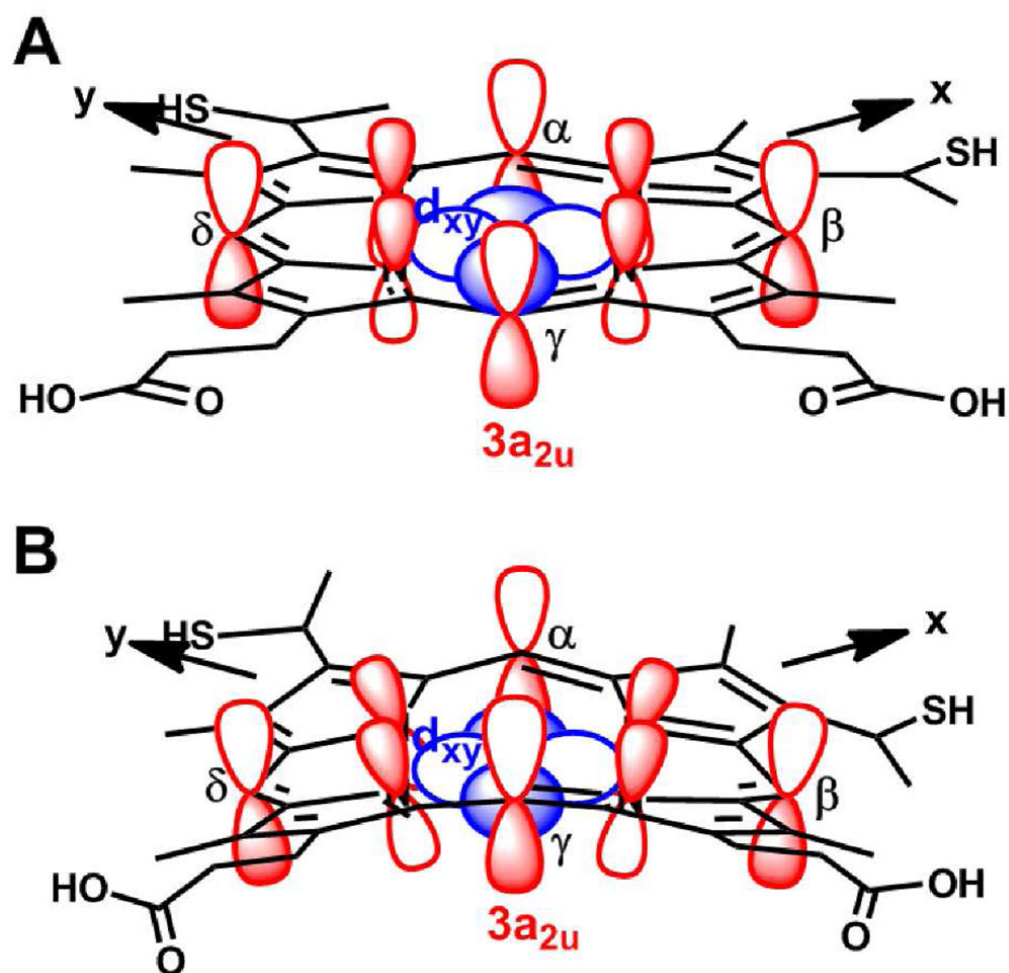


**Figure 8.** Illustration of the  $3a_{2u}$  orbital and the  $d_{xy}$  orbital in A) planar heme (interaction not allowed), and B) ruffled heme (interaction allowed).

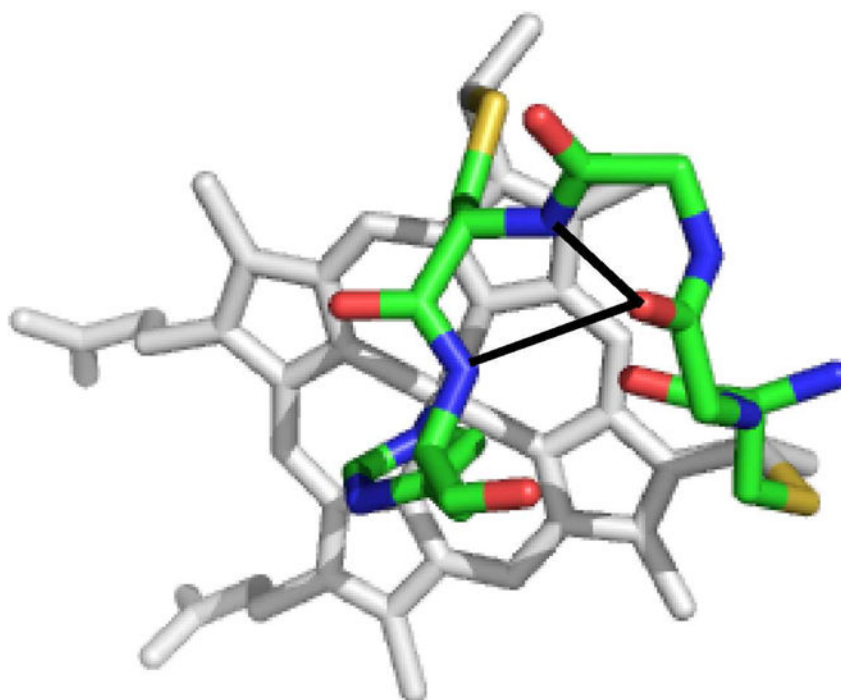


**Figure 9.** Structure of the heme and the residues 12–16 in *Ht c-552* (PDB: 1YNR).<sup>20</sup> The hydrogen-bonding interactions from Cys12(CO) to Cys15(HN) and His16 (HN) proposed to play a role in modulating CXXCH rigidity and heme ruffling are shown with black lines. The side chains of residues 13 and 14 are omitted for clarity.

**Table 1**

The  $g$ - and ligand-field ( $V$ ,  $\Delta$ ) values derived from low-temperature X-band EPR experiments. The symbol  $\xi$  indicates the spin-orbit coupling constant ( $\sim 400 \text{ cm}^{-1}$ ).

	$g_{\text{max}}$	$g_{\text{mid}}$	$g_{\text{min}}$	rhombic term $V/\lambda$	axial term $\Delta/\lambda$	rhombicity $V/\Delta$
<i>Ht c-552</i>	3.23	2.04	1.19	$1.23 \pm 0.02$	$3.41 \pm 0.06$	$0.36 \pm 0.01$
<i>HtK22M</i>	3.23	2.08	1.19	$1.24 \pm 0.02$	$3.23 \pm 0.08$	$0.38 \pm 0.01$
<i>HtM13V</i>	3.19	2.09	1.17	$1.26 \pm 0.02$	$3.06 \pm 0.10$	$0.41 \pm 0.01$
<i>HtM13V/K22M</i>	3.17	2.11	1.17	$1.28 \pm 0.01$	$2.96 \pm 0.06$	$0.43 \pm 0.01$
<i>Ht c-552</i>	$3.20^b$	$2.08^b$	$1.20^b$	$1.3 \pm 0.1^b$	$3.2 \pm 0.2^b$	$0.39 \pm 0.07^b$
<i>HtA7F</i>	$3.17^b$	$2.10^b$	$1.24^b$	$1.3 \pm 0.1^b$	$3.3 \pm 0.2^b$	$0.41 \pm 0.07^b$
<i>Pa c-551</i>	$3.20^b$	$2.06^b$	$1.23^b$	$1.28 \pm 0.02^b$	$3.45 \pm 0.03^b$	$0.37 \pm 0.01^b$
<i>PaF7A</i>	3.15	2.09	1.15	$1.26 \pm 0.02$	$2.94 \pm 0.05$	$0.43 \pm 0.01$

<sup>a</sup> data taken from ref. 18

<sup>b</sup> data taken from ref. 9, 16